Molecular Determinants of MAO Selectivity in a Series of Indolylmethylamine Derivatives: Biological Activities, 3D-QSAR/CoMFA Analysis, and Computational Simulation of Ligand Recognition

Jose A. Morón,[†] Mercedes Campillo,[#] Virgili Perez,[†] Mercedes Unzeta,*[,†] and Leonardo Pardo*[,#]

Laboratori de Medicina Computacional, Unitat de Bioestadistica, Facultat de Medicina, and Departament de Bioquímica i Biologia Molecular, Facultat de Medicina, Universitat Autònoma de Barcelona, 08193 Bellaterra, Barcelona, Spain

Received September 15, 1999

A series of indolylmethylamine derivatives were assayed toward MAO-A and MAO-B inhibition. The K_i values of these compounds are in the range from 0.8 to $>10^6$ nM for MAO-A or from 0.75 to 476000 nM for MAO-B. The most selective MAO-A or MAO-B inhibitors elicit a ratio of K_i in the order of 1500 or 1000, respectively. Comparison of MAO-A and MAO-B CoMFA models showed that both the steric and electrostatic properties at the 5 position of the indole ring are determinant for MAO selectivity. Computational simulations of the complex between this part of the ligand and Phe-208 of MAO-A or Ile-199 of MAO-B, experimentally identified as responsible for substrate selectivity, allowed us to further characterize the nature of these enzyme−inhibitor interactions.

Introduction

Molecular cloning,[1] substrate and inhibitor selectivity,[2,3] and tissue distribution[4] have led to the characterization of two isoforms of the mitochondrial flavin-containing monoamine oxidase (MAO), termed MAO-A and MAO-B, that catalyze the oxidative deamination of endogenous substances such as biogenic amines and neurotoxins.[5−7] The functional properties of MAO-A involve norepinefrine and serotonin as preferred substrates and clorgyline as irreversible inhibitor. In contrast, MAO-B prefers β-phenylethylamine and benzylamine as substrates and L-deprenyl as irreversible inhibitor. Mutagenesis experiments have identified a key amino acid responsible for substrate selectivity.[8] Substitution of Phe-208 in MAO-A by the corresponding Ile-199 in MAO-B converted the selectivity profile of MAO-A to MAO-B, and vice versa. Thus, aromatic interactions might be involved in MAO-A binding, whereas hydrophobic van der Waals' interaction might be involved in MAO-B binding.[8] Selective MAO-A inhibitors are used in the treatment of affective disorders,[9] and MAO-B inhibitors are valuable in the treatment of Parkinson's disease.[10]

Nevertheless, current understanding of MAO-A and MAO-B function is still hampered by the lack of detailed three-dimensional structures of these enzymes. Because their primary sequences do not share any sequence similarity with other proteins of known structure, structure−activity relationships can be useful in order to assess the structural properties of the ligands and the active sites of the enzymes required for molecular recognition (see refs 3 and 11−14 for several approaches). We have previously described that N-acetylenic and N-allenic derivatives of tryptamine act as effective and selective MAO inhibitors.[15−19] These studies showed the effect of different structural features in the selectivity and inhibitory potency of MAO. Here we report a three-dimensional quantitative structure−affinity relationship analysis (3D-QSAR),[20] using comparative molecular field analysis (CoMFA),[21] of a series of indolylmethylamine derivatives bearing substituents at N_1 and C_5 positions of the indole ring, to characterize the steric and electrostatic requirements needed at the active sites of the enzymes to explain the MAO-A/MAO-B selectivity. Subsequent simulations of the interaction of these inhibitors with protein models allowed us to further characterize the nature of these enzyme−inhibitor interactions.

Methods

3D-QSAR/CoMFA Method. The equilibrium structures of the protonated form of the indolylmethylamine derivatives were obtained by full geometry optimization with the AM-1 Hamiltonian model.[22] A critical step in CoMFA is the positioning of the molecules. The entire set of indolylmethylamine analogues was oriented in space by superimposing the heavy atoms of the common and rigid indole ring. The conformation of the *N*-alkylnyl side chain was chosen in such a way that the unsaturated moiety of all the structures had similar arrangement in space. K_i is a function of both the stabilization of the complexes formed between the ligand molecules and the enzyme and the solvation energy of the ligands. Thus, the QSAR table consists of the values of pK_i (dependent variable), the steric and electrostatic fields (independent variables), to mimic the stabilization energy of the enzyme−inhibitor complex, and the solvation energy (independent variable). The atom-centered atomic charges used in CoMFA to evaluate the electrostatic field were computed from the molecular electrostatic potential[23] using the 6-31G* basis set, a common procedure for the simulation of proteins, nucleic

* To whom correspondence should be addressed. For M.U.: phone, (3493) 581 1523; fax, (3493) 581 1573; e-mail, Mercedes.Unzeta@uab.es. For L.P.: phone, (3493) 581 2797; fax, (3493) 581 2344; e-mail, Leonardo.Pardo@uab.es.
[†] Departament de Bioquímica i Biologia Molecular.
[#] Laboratori de Medicina Computacional.

10.1021/jm991164x CCC: $19.00
Published on Web 04/13/2000

Table 1. Structures of the Indolylalkylamine Derivatives and Their Experimental (K_i and pK_i) and CoMFA Predicted (pK_i^{pred}) MAO-A and MAO-B Inhibitory Potencies

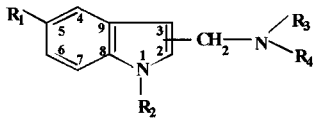

						MAO-A			MAO-B			pK_i(A) −
compd	R_1	R_2	*n*	R_3	R_4	K_i (μM)	pK_i (M)	pK_i^{pred} (M)	K_i (μM)	pK_i (M)	pK_i^{pred} (M)	pK_i(B)
FA26[a]	H−	CH_3−	2	H−	CH≡C−CH_2−	0.24	6.62[§]	6.44	3.83	5.42		1.20
FA27[a]	H−	CH_3−	2	CH_3−	CH≡C−CH_2−	0.0003	9.52[§]	9.31	0.003	8.52[§]	8.56	1.00
FA30[a]	H−	CH_3−	2	CH_3−	CH_3−C≡C−CH_2−	0.0043	8.37[§]	8.61	0.03	7.52[§]	7.48	0.85
FA102	HO−	CH_3−	2	H−	CH≡C−CH_2−	4.0	5.40[§]	5.54	8.9	5.05[§]	4.97	0.35
FA69	HO−	CH_3−	2	CH_3−	CH≡C−CH_2−	0.004	8.40[§]	8.59	0.82	6.09[§]	6.21	2.31
FA70	HO−	CH_3−	2	CH_3−	CH_3−C≡C−CH_2−	0.0057	8.24[§]	7.82	8.8	5.06[§]	5.04	3.18
FA42	CH_3O−	CH_3−	2	H−	CH≡C−CH_2−	0.0008	9.09		0.004	8.3		0.79
FA43[a]	CH_3O−	CH_3−	2	CH_3−	CH≡C−CH_2−	0.0015	8.82[§]	9.04	0.03	7.24[§]	7.23	1.58
FA45[a]	CH_3O−	CH_3−	2	CH_3−	CH_3−C≡C−CH_2−	0.0014	8.85	8.48[#]	0.37	6.43	6.26[#]	2.42
FA73[a]	C_6H_5−CH_2O−	H−	2	H−	CH≡C−CH_2−	0.79	6.10[§]	6.02	0.00075	9.12[§]	8.99	−3.02
FA74	C_6H_5−CH_2O−	H−	2	H−	CH_3−C≡C−CH_2−	5.25	4.82[§]	4.88	0.015	7.82[§]	7.94	−3.00
FA4	H−	H−	2	C_6H_5−CH_2−	H−	87	4.06[§]	4.06	159	3.80[§]	3.95	0.26
FA25	H−	CH_3−	2	C_6H_5−CH_2−	H−	34	4.47[§]	4.53	48	4.32[§]	4.37	0.15
FA28	H−	CH_3−	2	C_6H_5−CH_2−	CH≡C−CH_2−	10	5.00[§]	4.97	60	4.22		0.78
FA31	H−	CH_3−	2	C_6H_5−CH_2−	CH_3−C≡C−CH_2−	>1000			50	4.30[§]	4.14	
FA201	H−	C_6H_5−CH_2−	3	CH_3−	H−	167	3.78[§]	3.73	338	3.47[§]	3.39	0.31
FA202	H−	C_6H_5−CH_2−	3	CH_3−	CH≡C−CH_2−	160	3.80	4.65[#]	476	3.32	3.98[#]	0.48
FA203	H−	C_6H_5−CH_2−	3	CH_3−CH_2−	H−	262	3.58[§]	3.66	429	3.37[§]	3.36	0.21
FA205	H−	C_6H_5−CH_2−	3	$(CH_3)_2$−CH−	H−	133	3.88[§]	3.84	438	3.36[§]	3.27	0.52
FA207	H−	C_6H_5−CH_2−	3	C_6H_5−CH_2−	H−	244	3.61[§]	3.63	362	3.44[§]	3.49	0.17
FA208	H−	C_6H_5−CH_2−	3	C_6H_5−CH_2−	CH≡C−CH_2−	>1000			260	3.59[§]	3.69	

[a] Kinetic parameters previously described.[15,17,43] *n*: position of the side chain.

acids, and organic molecules.[24] The steric and electrostatic probe was a sp^3 carbon carrying a charge of +1.0. Solvation energies of the isolated indolylmethylamine derivatives were calculated with a polarized continuum model[25,26] using the 6-31G basis set. All the quantum mechanical calculations were performed with the GAUSSIAN-94 system of programs.[27] The CoMFA studies were carried out with the QSAR module of the SYBYL 6.3 program,[28] using default parameters.

A Model of Enzyme−Inhibitor Interaction. The interaction between Phe-208 in MAO-A and the corresponding Ile-199 in MAO-B with the 5 position of the indole ring was modeled by full geometry optimization at a level of theory (including MP2 treatment of electron correlation effects with the 6-31G* basis set) that is capable, in principle, of describing the proposed aromatic or van der Waals' interactions.[8] To characterize these interactions, a model system was constructed consisting of the side chains of Phe or Ile and the substituent at the 5 position bound to a benzyl ring. E_{int} represents the stabilization of the complex and is defined as the difference in energy between the fully optimized complex and the sum of the energies of the fully optimized isolated molecule and enzyme models. Solvation energies (E_{solv}) of the substituted benzyl ring were obtained by single-point calculation with a polarized continuum model[25,26] using the 6-31G* basis set at the MP2 level for consistency with the calculation of E_{int}. All the quantum mechanical calculations were performed with the GAUSSIAN-94 system of programs.[27]

Results and Discussion

MAO-A and MAO-B Inhibition. Table 1 shows the indolylmethylamine derivatives assayed for their inhibitory effect on MAO-A and MAO-B activities. The structural features studied include: (i) substitution at the 5 position of the indole ring (R_1) by HO−, CH_3O−, or C_6H_5−CH_2O−; (ii) substitution at the N_1 position of the indole ring (R_2) by CH_3− or C_6H_5−CH_2−; (iii) substitution at the positively charged nitrogen of the side chain (R_3) by CH_3−, CH_3−CH_2−, $(CH_3)_2$−CH−, or C_6H_5−CH_2−; and (iv) substitution at the positively charged nitrogen of the side chain (R_4) by CH≡C−CH_2− or CH_3−C≡C−CH_2−.

Substitution of the H atom at the 5 position of the indole ring (**FA26**) by HO− (**FA102**) diminishes the potency toward both MAO-A (0.24 μM for **FA26** versus 4 μM for **FA102**, see Table 1) and MAO-B (3.83 μM versus 8.9 μM) inhibition. In contrast, substitution at the same 5 position of the indole ring by CH_3O− (**FA42**) increases the potency toward both MAO-A (0.24 μM for **FA26** versus 0.0008 μM for **FA42**) and MAO-B (3.83 μM versus 0.004 μM) inhibition. Notably, the effect of adding a phenyl ring to the CH_3O− group, leading to the C_6H_5−CH_2O− substituent (**FA73**), has opposite effects in MAO-A and MAO-B inhibition. It decreases the potency toward MAO-A (0.0008 μM versus 0.79 μM for **FA42** and **FA73**, respectively), and it increases the potency toward MAO-B (0.004 μM versus 0.00075 μM, respectively). Clearly, this opposite effect provides the desired selectivity of **FA73** toward the MAO-B isoform with a ratio of potencies in the order of 1000 times. These two compounds **FA42** and **FA73** are the most potent MAO-A and MAO-B inhibitors, respectively, in this series of indolylmethylamine derivatives of tryptamine.

The effect of adding a C_6H_5−CH_2− group to the N_1 nitrogen of the indole ring (**FA201, FA202, FA203, FA205, FA207,** and **FA208**) produces a dramatic drop in affinity toward both MAO isoform inhibition. The K_i values are in the range 160−262 μM for MAO-A (with

the exception of **FA208** which has no inhibitory effect at a concentration of 1000 μM) or 260−476 μM for MAO-B inhibition.

The K_i values of compounds **FA4, FA25, FA28,** and **FA31**, where a $C_6H_5-CH_2-$ group has been attached to the positively charged nitrogen of the side chain, are in the range 10−87 μM for MAO-A (with the exception of **FA31** which has no inhibitory effect at a concentration of 1000 μM) or 48−159 μM for MAO-B inhibition.

Finally, addition of the CH_3- group to the $CH\equiv C-CH_2-$ substituent of the positively charged nitrogen, leading to the $CH_3-C\equiv C-CH_2-$ group, diminishes the affinity toward MAO inhibition. The effect of this addition in the MAO-B inhibition (monitored by the ratio of K_i values) is almost constant: 10.0 for **FA27** versus **FA30** that contain a 5-H-indole ring, 10.7 for **FA69** versus **FA70** that contain a 5-OH-indole ring, 7.5 for **FA43** versus **FA45** that contain a 5-OCH_3-indole ring, or 20.0 for **FA73** versus **FA74** that contain a 5-OCH_2-C_6H_5-indole ring. In contrast, the change in MAO-A inhibition is not of the same magnitude for all comparisons. The ratio of MAO-A inhibitory constants for the 5-H (14.3, **FA27** versus **FA30**) and 5-OCH_2-C_6H_5 (6.7, **FA73** versus **FA74**) comparisons is in the range obtained for MAO-B inhibition, whereas the effect of the CH_3- addition is very small for the 5-OH (1.4, **FA69** versus **FA70**) and 5-OCH_3 (0.9, **FA43** versus **FA45**) comparisons. These findings suggest that there might be a small cavity present only in the active center of the MAO-A isoform. The orientation of **FA45** and **FA70** in the active center of MAO-A, guided by the interaction of the 5-OH and 5-OCH_3 moieties, might allow the methyl group to be accommodated inside this cavity. Clearly, **FA70** is the most selective compound toward the MAO-A isoform with a ratio of potencies of 1500 times.

3D-QSAR/CoMFA Models. The method of systematically adding bulky substituents at different positions of the molecules will allow us to characterize the steric requirements needed for enzyme selectivity. Thus, the inhibitory potencies (pK_i) against both MAO-A and MAO-B substrates of the set of compounds marked with § in Table 1 were related to the independent variables (steric and electrostatic fields and solvation energy) by the partial least-squares (PLS) methodology.[29,30] Compound **FA42** was not included in the MAO-A CoMFA model; compounds **FA42, FA26,** and **FA28** were not included in the MAO-B CoMFA model because their residuals were the highest and greater than two standard deviations. Clearly, the steric and electrostatic fields cannot reproduce the type of interaction between **FA42**, one of the most potent MAO inhibitors, and the active center of the enzyme, required to elicit such a potency. More accurate methods, based on ab initio quantum mechanical calculations (see "A Model of Enzyme−Inhibitor Interaction", below), are employed to explain the inhibitory properties of **FA42**. In addition, randomly chosen compounds (**FA45** and **FA202**) were not included in the initial set in order to test the predictive power of the derived CoMFA models on these ligands. Table 2 shows the obtained statistical parameters. The relative contributions of the steric, electrostatic, and solvation terms follow similar trends in the MAO-A (55.3:31.5:13.3, respectively) and MAO-B (55.9:31.2:12.9) CoMFA models. From a statistical viewpoint, the high values of the obtained cross-validated correlation coefficient q^2 (0.895 and 0.859 for MAO-A and MAO-B, respectively) reveal that both models are useful tools for predicting the biological activity. As a further test of robustness, the CoMFA models were applied to the omitted **FA45** and **FA202** ligands. Clearly, the theoretically predicted pK_i values (see the # symbol in Table 1) are in an acceptable agreement with the experimentally determined values. The theoretically predicted and experimentally determined pK_i values, for the whole set of compounds, are listed in Table 1 and plotted in Figure 1.

Table 2. Statistical Results of MAO-A and MAO-B CoMFA Models

	MAO-A	MAO-B
$q^{2\,a}$	0.895	0.859
N^b	6	6
n^c	16	16
$r^{2\,d}$	0.993	0.998
F	220.866	674.083
steric[e]	55.3	55.9
electrostatic[e]	31.5	31.2
solvation[e]	13.3	12.9

[a] Cross-validated correlation coefficient. [b] Optimal number of principal components. [c] Number of compounds. [d] Non-cross-validated correlation coefficient. [e] Percentage of contribution.

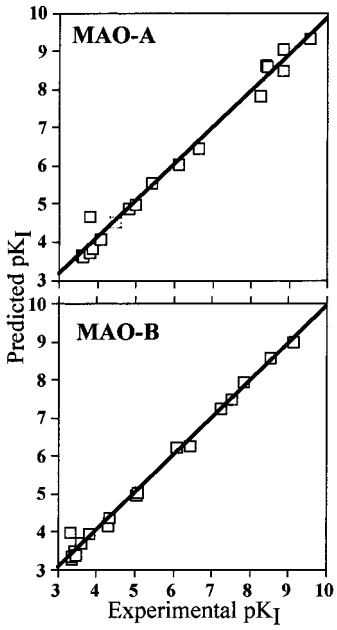

Figure 1. Plot of the predicted pK_i versus the experimental pK_i values for the MAO-A ($n = 18$, $r = 0.992$, $s = 0.277$, $p < 0.0001$) and MAO-B ($n = 18$, $r = 0.996$, $s = 0.188$, $p < 0.0001$) CoMFA models.

Figures 2 and 3 depict the CoMFA electrostatic and steric maps using compounds **FA70** and **FA73**, the most selective MAO-A and MAO-B compounds, respectively, as the reference structures. The color code of the electrostatic maps (Figure 2) is as follows: areas where a high electron density provided by the ligand increases (red) or decreases (blue) the binding affinity. The CoMFA electrostatic maps for MAO-A and MAO-B are very similar in the side chain moiety. The volume in the proximity of the indole ring of the molecule is the only part where divergences can be found between both maps (see Figure 2). First, the red area near the

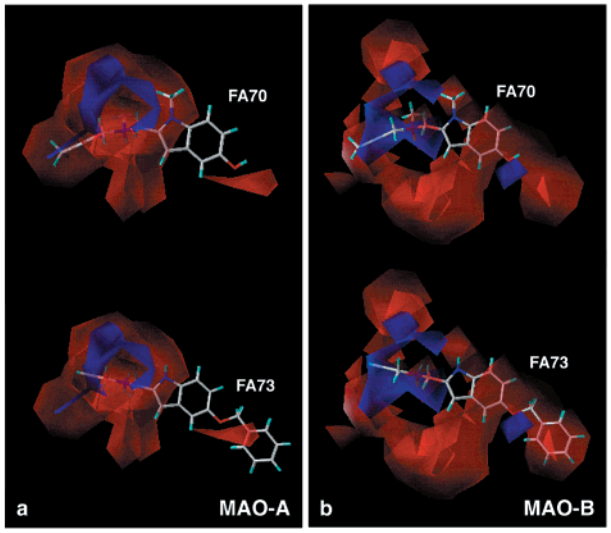

Figure 2. Electrostatic maps from the (a) MAO-A and (b) MAO-B CoMFA models for MAO inhibition. Compounds **FA70** and **FA73** are shown as the reference structures. The color code is as follows: areas where a high electron density provided by the ligand increases (red) or decreases (blue) the binding affinity.

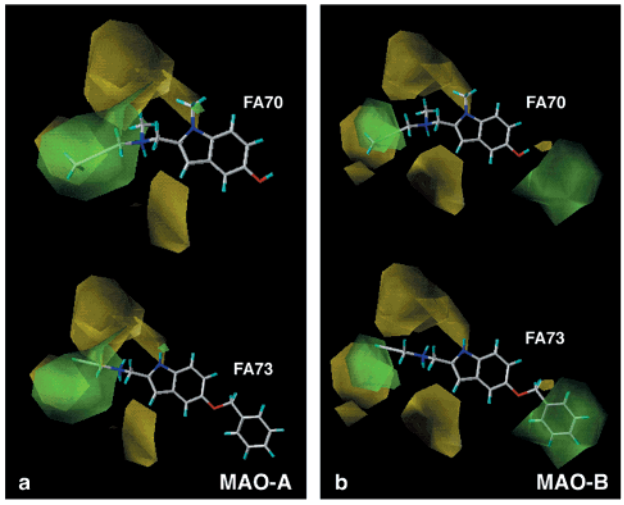

Figure 3. Steric maps from the (a) MAO-A and (b) MAO-B CoMFA models for MAO inhibition. Compounds **FA70** and **FA73** are shown as the reference structures. The color code is as follows: green areas depict zones of space where occupancy by the ligands increases affinity, whereas yellow areas depict zones where occupancy decreases affinity.

substituent at the 5 position of the indole ring, in the MAO-A model, contrasts with the blue area, in the MAO-B model. Thus, opposite electrostatic properties are required, at this part of the molecule, for molecular recognition by the MAO isoforms. Second, the MAO-B electrostatic map possesses a unique red area that extends throughout the indole ring and the aromatic ring of the $C_6H_5-CH_2O-$ substituent of **FA73**. Thus, the significant potency of **FA73** is probably achieved by the interaction between the π electron-rich clouds of the aromatic rings and the MAO-B active center. Moreover, the absence of this red area in the MAO-A map explains the observed selectivity of **FA73** toward the MAO-B isoform.

The color code of the steric maps (Figure 3) is as follows: green areas depict zones of space where occupancy by the ligands increases affinity, whereas yellow areas depict zones where occupancy decreases affinity. The yellow area located at the upper-left side of the figure indicates that bulky substituents at the N_1 position of the indole ring are not tolerated in both MAO-A and MAO-B active centers. The green area found in the proximity of the unsaturated moiety is more extensive in the MAO-A map than in the MAO-B map. Furthermore, yellow areas surround this green area in both maps. Remarkably, the CH_3- moiety of the $CH_3-C\equiv C-CH_2-$ group of **FA70** is accommodated inside the green area in the MAO-A map, whereas this CH_3- group partially contacts the yellow area in the MAO-B map. These findings are in good agreement with the previous hypothesis (see "MAO-A and MAO-B Inhibition", above) that there might be a small cavity present only in the active center of the MAO-A isoform in which the CH_3- group accommodates. However, the most salient difference between the MAO-A and MAO-B maps resides at the 5 position of the indole ring. The unique and extensive green area in the MAO-B map indicates that bulky substituents at this 5 position are beneficial for MAO-B binding. Thus, addition of a phenyl ring to the CH_3O- group (**FA42**), leading to the $C_6H_5-CH_2O-$ substituent (**FA73**), is clearly favorable (0.004 μM versus 0.00075 μM; see above, Table 1, and Figure 3). In contrast, the absence of this area in the MAO-A map suggests that this substitution does not enhance affinity for the MAO-A isoform.

Comparison of the MAO-A and MAO-B CoMFA maps leads to the main conclusion that the 5 position of the indole ring is involved in the MAO-A/MAO-B selectivity: (i) the steric requirements at the MAO-A active site are more restricted, at this position, than at the MAO-B active site and (ii) different electrostatic properties, at the indole ring region, are required for molecular recognition by the MAO isoforms.

A Model of Enzyme−Inhibitor Interaction. Mutagenesis experiments on MAO isoforms have identified the importance of Phe-208 in MAO-A and the corresponding Ile-199 in MAO-B for substrate selectivity.[8] As noted by the same authors, the different physicochemical properties of these aromatic and aliphatic side chains are responsible for substrate selectivity. We can assume, as a working hypothesis, that the reported MAO inhibitors bind to the same active site as substrates do and act by blocking the access of the substrate to the active site. Thus, the steric and electrostatic characteristics of the CoMFA maps (see above) led us to propose the interaction of the indole ring and the substituent at the 5 position with the side chain of either Phe-208 or Ile-199. Moreover, this aromatic ring is a common moiety of the substrates used in the mutagenesis experiments.[8] To identify the arrangement in space of these essential determinants for selective recognition, we performed full geometry optimization (see Methods section for computational details) of a benzyl ring substituted by HO− (as a model of **FA102**), CH_3O- (**FA42**), or $C_6H_5-CH_2O-$ (**FA73**) and the side chains of Phe or Ile. It is important to note that in order to properly describe these proposed interactions it is necessary to include correlation effects in the calculations. Thus, geometry optimization at the MP2/6-31G*

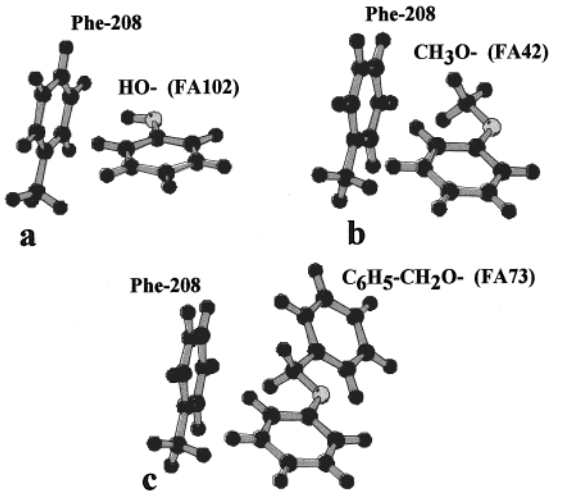

Figure 4. Detailed view of Phe-208 (MAO-A) in its interaction with a benzyl ring substituted by (a) HO− (as a model of **FA102**), (b) CH_3O- (**FA42**), or (c) $C_6H_5-CH_2O-$ (**FA73**). The figure was created using MOLSCRIPT.[48]

level of theory of these minimal recognition models represents a significant computational effort.

Figure 4 presents a detailed view of Phe-208 (MAO-A) in its interaction with the substituted HO− (Figure 4a) and CH_3O- (Figure 4b) benzyl ring. The Phe-208 side chain is positioned in the face-to-edge orientation (T-shaped) to the substituted benzyl ring. The hydrogen bond[31] is formed between the π electron-rich clouds of the aromatic Phe ring and the electron-poor hydrogens of the ligand in a manner similar to the proposed hydrogen bond between benzene and water.[32] This type of aromatic−aromatic interaction has also been described as a mechanism of protein structure stabilization.[33] Table 3 shows the energy of interaction, E_{int}, of the ligand−enzyme complexes. The value of −7.2 kcal/mol for **FA102** is larger than the value of −5.4 kcal/mol for **FA42**. Thus, the hydrogen bond between the more polar HO− group (**FA102**) and Phe-208 is stronger than the two C−H groups of CH_3O- (**FA42**) pointing toward Phe-208 (see Figure 4). Calculations such as those described for the OH- and CH_3O-substituted benzyl ring become inviable for the $C_6H_5-CH_2O-$ substituent (**FA73**) due to the large number of basis functions and the calculation of correlation energy. Thus, the optimal geometry of interaction between the $C_6H_5-CH_2O$-substituted phenyl ring and Phe-208 must be carried out in two optimization steps. First, the relative position of the common atoms of Phe-208, the $-CH_2O-$ moiety, and the benzyl ring is taken from that previously obtained with the CH_3O- substituent (see Figure 4b). Second, the position of the other noncommon atoms (the C_6H_5- moiety) was optimized at the MP2/6-31G* level, keeping Phe-208 and the $-CH_2O-$ moiety fixed, in the absence of the benzyl ring. Figure 4c depicts the final obtained structure of the complex. The value of E_{int} of −5.3 kcal/mol (see Table 3) reveals that addition of the C_6H_5- group does not improve the interaction of the ligand with Phe-208.

It is desirable to compare the experimental difference of formation free energies between the complex with **FA102** and with a given ligand ($\Delta\Delta G_f^{\mathbf{FA102}/\text{ligand}}$), evaluated from the ratio of inhibitory constants ($K_i^{\mathbf{FA102}}/K_i^{\text{ligand}}$), with the theoretically predicted values (see Table 3). It is difficult to evaluate these free energy differences, by computational methods, without knowing the tertiary structure of the enzyme (see ref 34 for free energy perturbation details). However, $\Delta\Delta G_f^{\mathbf{FA102}/\text{ligand}}$ can be estimated from the difference of formation enthalpies, $\Delta\Delta H_f^{\mathbf{FA102}/\text{ligand}}$, if cancellation of entropic effects is assumed. This assumption is reasonable because there are not major differences in the process of ligand binding. Moreover, the difference of formation enthalpies can be determined as:[35]

$$\Delta\Delta H_f^{\mathbf{FA102}/\text{ligand}} = \Delta H_f^{\text{ligand}} - \Delta H_f^{\mathbf{FA102}} = (E_{int}^{\text{ligand}} - E_{solv}^{\text{ligand}}) - (E_{int}^{\mathbf{FA102}} - E_{solv}^{\mathbf{FA102}})$$

where E_{solv} is the energy obtained by solvating the ligand and E_{int} is the interaction energy of the complex formed between the ligand molecule and the enzyme model. It is important to note that the enthalpy of formation, ΔH_f, does not describe the process of ligand binding because (i) models of both the ligand and the enzyme have been considered in the calculations and (ii) the conformational and solvation changes in the tertiary structure of the enzyme, following ligand binding, have not been taken into account, among others. Nevertheless, the difference in the values of enthalpies of formation, $\Delta\Delta H_f^{\mathbf{FA102}/\text{ligand}}$, is suitable to understand the experimental rank order of potencies, if the above-mentioned approximations are assumed to affect all ligands equally. Table 3 shows the experimental $\Delta\Delta G_f^{\mathbf{FA102}/\text{ligand}}$ and theoretical $\Delta\Delta H_f^{\mathbf{FA102}/\text{ligand}}$ for the MAO-A isoform. Notably, the predicted order of MAO-A

Table 3. For the **FA102**, **FA42**, and **FA73** Ligands: Experimental Inhibitory Potencies, K_i (μM); Experimental Difference of Formation Free Energies between **FA102** and a Given Ligand, $\Delta\Delta G_f$ (kcal/mol); Calculated Energies of Interaction, E_{int} (kcal/mol), of the Ligand−Enzyme Complex; Calculated Energies of Solvation, E_{solv} (kcal/mol), of the Isolated Ligands; Predicted Difference of Formation Enthalpies, $\Delta\Delta H_f$ (kcal/mol); Experimental Ratio of Inhibitory Potencies between MAO Enzymes, K_i^{MAO-B}/K_i^{MAO-A}; Experimental Difference of Formation Free Energies between MAO Enzymes, $\Delta\Delta G_f^{B/A}$ (kcal/mol); and Predicted Difference of Formation Enthalpies between MAO Enzymes, $\Delta\Delta H_f^{B/A}$ (kcal/mol)

	FA102 OH−	**FA42** CH_3O-	**FA73** $C_6H_5-CH_2O-$
E_{solv}[a]	−7.4	−2.0	−4.6
MAO-A Inhibition			
E_{int}[b]	−7.2	−5.4	−5.3
K_i	4.1	0.0008	0.79
$\Delta\Delta G_f^{\mathbf{FA102}/\text{ligand}}$ [c]		−5.2	−1.0
$\Delta\Delta H_f^{\mathbf{FA102}/\text{ligand}}$ [d]		−3.6	−0.9
MAO-B Inhibition			
E_{int}[b] complex i	−2.8	−3.3	
E_{int}[b] complex ii	−4.4	−4.5	−7.2
K_i	8.9	0.004	0.00075
$\Delta\Delta G_f^{\mathbf{FA102}/\text{ligand}}$ [c]		−4.7	−5.8
$\Delta\Delta H_f^{\mathbf{FA102}/\text{ligand}}$ [d]		−5.5	−5.6
MAO-A/MAO-B Selectivity			
K_i^{MAO-B}/K_i^{MAO-A}	2.2	5.0	0.0009
$\Delta\Delta G_f^{B/A}$ [e]	−0.5	−1.0	4.3
$\Delta\Delta H_f^{B/A}$ [f]	−2.8	−0.9	1.9

[a] Single-point calculation at the MP2/6-31G* level with a polarized continuum model.[33,34] [b] Calculated at the MP2/6-31G*//MP2/6-31G* level of theory. [c] Calculated as $\Delta\Delta G_f = -0.616 \ln(K_i^{\mathbf{FA102}}/K_i^{\text{ligand}})$. [d] Calculated as $\Delta\Delta H_f = (E_{int}^{\text{ligand}} - E_{solv}^{\text{ligand}}) - (E_{int}^{\mathbf{FA102}} - E_{solv}^{\mathbf{FA102}})$. [e] Calculated as $\Delta\Delta G_f = -0.616 \ln(K_i^{MAO-B}/K_i^{MAO-A})$. [f] Calculated as $\Delta\Delta H_f = E_{int}^{MAO-A} - E_{int}^{MAO-B}$.

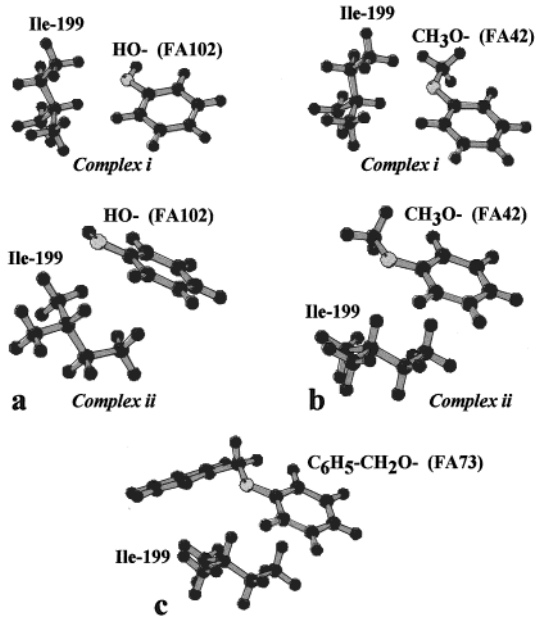

Figure 5. Detailed view of Ile-199 (MAO-B) in its interaction with a benzyl ring substituted by (a) HO− (as a model of **FA102**), (b) CH_3O- (**FA42**), or (c) $C_6H_5-CH_2O-$ (**FA73**). Complex i denotes a mode of interaction in which the electron-poor C^{β}-H and C^{δ}-H hydrogens of Ile-199 form a hydrogen bond to the electron-rich O atom of the HO− or CH_3O- substituent. Complex ii denotes a mode of interaction in which the C^{β}-H group forms a hydrogen bond to the O atom of the HO− or CH_3O- substituent and the C^{δ}-H group forms a hydrogen bond with the π electrons clouds of the aromatic benzyl ring.

inhibitory potencies ($\Delta\Delta H_f$ of −3.6 and −0.9 kcal/mol for **FA42** and **FA73**, respectively) reproduces the experimental rank order ($\Delta\Delta G_f$ of −5.2 and −1.0 kcal/mol for **FA42** and **FA73**, respectively). Thus, substitution of the HO− group at the 5 position of the indole ring (**FA102**) by CH_3O- (**FA42**) significantly decreases the energy penalty to desolvate the ligand (−7.4 versus −2.0 kcal/mol, respectively). The stronger interaction of HO− than CH_3O- with Phe-208 (−7.2 versus −5.4 kcal/mol, respectively) does not compensate the energy cost of desolvating the HO-substituted ligand. This results in a noticeable increase in the potency of **FA42**. On the other hand, the $C_6H_5-CH_2O-$ substituent (**FA73**) possesses solvation energies between **FA102** and **FA42** and an interaction energy with Phe-208 of the same order as that of **FA42** (see Table 3). In consequence, **FA73** is a ligand with moderate potency toward MAO-A inhibition.

Figure 5 presents a detailed view of Ile-199 (MAO-B) in its interaction with the substituted HO− (Figure 5a) and CH_3O- (Figure 5b) benzyl ring. Two possible ligand−enzyme complexes are reported: Complex i denotes a mode of interaction in which the electron-poor C^{β}-H and C^{δ}-H hydrogens of Ile-199 form a hydrogen bond to the electron-rich atom of the HO− or CH_3O- substituent. This type of C−H···O hydrogen bond has recently been reported in protein−DNA recognition,[36] in the stability of Pro residues in α-helices,[37] and in protein structure stabilization.[38] Complex ii denotes a mode of interaction in which the C^{β}-H group forms a hydrogen bond to the O atom of the HO− or CH_3O- substituent and the C^{δ}-H group forms a hydrogen bond with the π electrons clouds of the aromatic benzyl ring (or indole ring in the complete structure of the ligand). This type of C−H···π interaction has been reported in the packing of the aromatic ring of adenine in protein structures.[39] Table 3 reports the energies of interaction of both complexes. Thus, complex ii possesses lower energy than complex i. However, given the small difference in energy (−2.8 versus −4.4 kcal/mol for HO− and −3.3 versus −4.5 kcal/mol for CH_3O-) the orientation of the side chain imposed by the secondary structure to which this residue is bound might reverse or increase this energy preference. Though we cannot discriminate between both complexes, we will consider complex ii as the recognition model for the interaction with Ile-199 given its lower energy. Figure 5c shows the final obtained structure of the complex with the $C_6H_5-CH_2O-$substituted phenyl ring (see above for the optimization process). The electron-poor C-H hydrogens of Ile-199 interact with the π electron-rich clouds of both aromatic rings. The value of E_{int} of −7.2 kcal/mol (see Table 3) reveals that addition of a supplementary aromatic ring (the C_6H_5- group) allows **FA73** to efficiently bind Ile-199 throughout several weak hydrogen bonds. The red area found in the MAO-B electrostatic map of the CoMFA model (see above and Figure 2) was thus reflecting the importance of the π electron-rich clouds of the aromatic rings for enzyme binding. Similarly, the unique green area in the MAO-B steric map of the CoMFA model (see Figure 3), at the position of the C_6H_5- group of the $C_6H_5-CH_2O-$ substituent, was reflecting the additional interaction of this ring with Ile-199.

Table 3 shows the experimental $\Delta\Delta G_f^{\mathbf{FA102}/\text{ligand}}$ and theoretical $\Delta\Delta H_f^{\mathbf{FA102}/\text{ligand}}$ for the MAO-B isoform. Notably, the predicted order of MAO-B inhibitory potencies ($\Delta\Delta H_f$ of −5.5 and −5.6 kcal/mol for **FA42** and **FA73**, respectively) reproduces quantitatively the experimental rank order ($\Delta\Delta G_f$ of −4.7 and −5.8 kcal/mol for **FA42** and **FA73**, respectively). The higher energy penalty required to desolvate the HO− substituent compared to the CH_3O- substituent explains the lower potency of **FA102** compared with **FA42** toward MAO-B, in an analogous manner to the MAO-A interaction (see above). The energy penalty to desolvate the $C_6H_5-CH_2O-$substituted benzyl ring (**FA73**, −4.6 kcal/mol) is greater than for the CH_3O- substituent (**FA42**, −2.0 kcal/mol). However, this energy is compensated by the stronger interaction with Ile-199 (−4.5 versus −7.2 kcal/mol for **FA42** and **FA73**, respectively). These results explain the mechanism by which **FA73** is the most potent MAO-B inhibitor presented in this work.

Finally, Table 3 shows the experimental ratio of inhibitory potencies between MAO enzymes, K_i^{MAO-B}/K_i^{MAO-A}; the experimental difference of formation free energies between MAO enzymes, $\Delta\Delta G_f^{B/A}$; and the predicted difference of formation enthalpies between MAO enzymes, $\Delta\Delta H_f^{B/A}$, for the **FA102, FA42,** and **FA73** ligands. The interaction of the OH- (**FA102**) or CH_3O- (**FA42**) substituted benzyl ring with Phe-208 of MAO-A (−7.2 and −5.4 kcal/mol, respectively) is higher than with Ile-199 of MAO-B (−4.4 and −4.5 kcal/mol). Thus, the theoretical values of $\Delta\Delta H_f^{B/A}$ of −2.8 kcal/mol for **FA102** and −0.9 kcal/mol for **FA42** reproduce the observed selectivity of these compounds toward the MAO-A enzyme. In contrast, the interaction of the $C_6H_5-CH_2O-$substituted benzyl ring (**FA73**) with Phe-

208 (−5.3 kcal/mol) is lower than with Ile-199 (−7.2 kcal/mol). Thus, the high selectivity profile of **FA73** toward the MAO-B isoform is explained by the different interaction energy with Phe and Ile residues.

Conclusions

3D-QSAR/CoMFA analysis and computational simulations of ligand recognition have been successfully applied to explain the inhibitory potencies of a series of indolylmethylamine derivatives toward the MAO-A and MAO-B isoforms. The most selective compounds elicit a ratio of inhibitory potencies in the order of 1500 for MAO-A or 1000 for MAO-B. Both derived computational models have facilitated the identification of the structural elements of the ligands that are key to explain the observed selectivity. Notably, the common indole ring of these compounds acts with different electrostatic properties toward the MAO-A active center (throughout the electron-poor hydrogens of the ring) than toward the MAO-B active center (throughout the π electron-rich clouds of the ring). These findings provide the tools for predicting the biological activity of untested compounds and designing new selective ligands.

Experimental Section

Chemicals. 5-Hydroxy[*side-chain-2*-^{14}C]tryptamine creatinine sulfate (55 mCi/mmol, 50 μCi/mL) was purchased from Amersham (U.K.). [*ethyl-1*-^{14}C]Phenylethylamine (50 mCi/mmol, 0.1 mCi/mL) was purchased from New England Nuclear (U.K.). Kynuramine dihydrobromide, benzylamine HCl, L-deprenyl and clorgyline were obtained from Sigma Chemical Co. (U.K.). The series of indolylmethylamine derivatives used in this study were synthesized by Cruces et al.[40]

MAO-A and MAO-B Inhibition Kinetic Studies. Rat liver mitochondrial fraction from male Sprague−Dawley rats (200−250 g) was prepared by a standard differential centrifugation method.[41] Liver homogenates were prepared in 10 vol (w/v) of a 50 mM potassium phosphate buffer (pH 7.2) by use of a Dounce homogenizer. MAO activities were determined radiochemically[42] using [^{14}C]5HT (100 μM) and [^{14}C]PEA (20 μM) as specific substrates for MAO-A and MAO-B, respectively. IC_{50} values were determined with and without preincubation of the inhibitor with the enzyme for 30 min at 37 °C. Previous studies indicated that the acetylenic indolylmethylamine derivatives behave as mechanism-based inhibitors of MAO,[15−19,43] whereas their corresponding parent amines behave as competitive inhibitors of MAO.[17]

The mechanism-based inhibition was quantified by a modification of the Walker and Elmore method[44] previously reported.[16] The kinetic constants defining the reversible complex formation (K_i) and the covalent adduct formation (k_{inact})

$$E + I \overset{K_i}{\rightleftharpoons} E\cdots I \overset{k_{inact}}{\rightleftharpoons} E-I$$

were determined by direct analysis of the reaction progress curves obtained spectrophotometrically in the presence of varying concentrations of inhibitor. MAO-B activity was obtained at 37 °C using 333 μM benzylamine as a specific substrate by measuring the appearance of the product at 250 nm by a modification[16] of the Tabor method.[45] MAO-A activity was determined spectrophotometrically using 40 μM kynuramine as a substrate[46] by measuring the appearance of the product at 324 nm.[16] Since kynuramine is a common substrate of both MAO forms, it was necessary beforehand to inhibit MAO-B activity with 3×10^{-7} L-deprenyl.

On the other hand, the kinetic constants of the competitive inhibition (K_i) of the parent amines were determined from the IC_{50} values by the Cheng−Prusoff equation:[47] $K_i = IC_{50}/(1 + [S]/K_m)$.

Acknowledgment. This work was supported in part by grants from CICYT: SAF99-073 (L.P.) and SAF99-093 (M.U.) and Fundació La Marató TV3: 0014/97 (L.P.). Some of the simulations were run at the Centre de Computació i Comunicacions de Catalunya.

References

(1) Bach, A. W. J.; Lan, N. C.; Johnson, D. L.; Abell, C. W.; Bembenek, M. E.; Kwan, S.-W.; Seeburg, P. H.; Shih, J. C. cDNA cloning of human liver monoamine oxidase A and B: Molecular basis of differences in enzymatic properties. *Proc. Natl. Acad. Sci. U.S.A.* **1988**, *85*, 4934−4938.

(2) Johnston, J. P. Some observations upon a new inhibitor of monoamine oxidase in brain tissue. *Biochem. Pharmacol.* **1968**, *17*, 1285−1297.

(3) Kalgutkar, A. S.; Castagnoli, N. J.; Testa, B. Selective inhibitors of monoamine oxidase (MAO-A and MAO-B) as probes of its catalytic site and mechanism. *Med. Res. Rev.* **1995**, *15*, 325−389.

(4) Westlund, R. N.; Denney, R. M.; Kochersperger, L. M.; Rose, R. M.; Abell, C. W. Distinct monoamine oxidase A and B populations in primate brain. *Science* **1985**, *230*, 181−183.

(5) Langston, J. W.; Ballard, P.; Tetrud, J. W.; Irwin, I. Chronic Parkinsonism in humans due to a product of meperidine-analogue synthesis. *Science* **1983**, *219*, 979−980.

(6) Salach, J. I.; Singer, T. P.; Castagnoli, N. J.; Trevor, A. Oxidation of the neurotoxic amine 1-methyl-4-phenyl-1,2,3,6-tetrahydropyridine (MPTP) by monoamine oxidases A and B and suicide inactivation of the enzymes by MPTP. *Biochem. Biophys. Res. Commun.* **1984**, *125*, 831−835.

(7) Singer, T. P. Perspectives in MAO: past, present, and future. A review. *J. Neural Transm. Suppl.* **1987**, *23*, 1−23.

(8) Tsugeno, Y.; Ito, A. A Key Amino Acid Responsible for Substrate Selectivity of Monoamine Oxidase A and B. *J. Biol. Chem.* **1997**, *272*, 14033−14036.

(9) Tipton, K. F. In *Biochemical and Pharmacological Aspects of Depression*; Tipton, K. F., Youdim, M. B. H., Eds.; Taylor and Francis: London, 1989; pp 1−24.

(10) Tetrud, V. W.; Langstron, J. W. The effect of deprenyl (selegiline) on the natural history of Parkinson's disease. *Science* **1989**, *245*, 519.

(11) Efange, S. M. N.; Boudreau, R. J. Molecular determinants in the bioactivation of the dopaminergic neurotoxin *N*-methyl-4-phenyl-1,2,3,6-tetrahydropyridine (MPTP). *J. Comput.-Aided Mol. Des.* **1991**, *5*, 405−417.

(12) Kneubühler, S.; Thull, U.; Altomare, C.; Carta, V.; Gaillard, P.; Carrupt, P. A.; Carotti, A.; Testa, B. Inhibition of Monoamine Oxidase-B by 5H-Indeno[1,2-c]pyridazines: Biological Activities, Quantitative Structure−Activity Relationships (QSARs) and 3D-QSARs. *J. Med. Chem.* **1995**, *38*, 3874−3883.

(13) Palmer, S. L.; Mabic, S.; Castagnoli, N. J. Probing the Active Sites of Monoamine Oxidase A and B with 1,4-Disubstituted Tetrahydropyridine Substrates and Inactivators. *J. Med. Chem.* **1997**, *40*, 1982−1989.

(14) Wang, Y. X.; Mabic, S.; Castagnoli, N. J. 1-Methyl-3-pyrrolines and 2-methylisoindolines: new classes of cyclic tertiary amine monoamine oxidase B substrates. *Bioorg. Med. Chem.* **1998**, *6*, 143−149.

(15) Balsa, M. D.; Fernández-Alvarez, E.; Tipton, K. F.; Unzeta, M. Inhibition of MAO by substituted tryptamine analogues. *J. Neural Transm. Suppl.* **1990**, *32*, 103−105.

(16) Avila, M.; Balsa, M. D.; Fernández-Alvarez, E.; Tipton, K. F.; Unzeta, M. The effect of side chain substitution at positions 2 and 3 of the heterocyclic ring of *N*-acetylenic analogues of tryptamine as monoamine oxidase inhibitors. *Biochem. Pharmacol.* **1993**, *45*, 2231−2237.

(17) Balsa, M. D.; Pérez, V.; Fernández-Alvarez, E.; Unzeta, M. Kinetic behavior of some acetylenic indolalkylamine derivatives and their corresponding parent amines. *J. Neural Transm. Suppl.* **1994**, *41*, 281−285.

(18) Pérez, V.; Marco, J. L.; Fernández-Alvarez, E.; Unzeta, M. Kinetic studies of N-allenic analogues of tryptamine as monoamine oxidase inhibitors. *J. Pharm. Pharmacol.* **1996**, *48*, 718−722.

(19) Morón, J. A.; Pérez, V.; Marco, J. L.; Fernandez-Alvarez, E.; Unzeta M. New 2-[(5-methoxy-1-methylindolyl)]-alkylamine derivatives: the effect of branching and elongation of the side chain on MAO inhibition. *J. Enzymol. Inhib.* **1998**, *13*, 237−251.

(20) Green, S. M.; Marshall, G. R. 3D-QSAR: a current perspective. *Trends Pharmacol. Sci.* **1995**, *16*, 285−291.

(21) Cramer, R. D.; Patterson, D. E.; Bunce, J. D. Comparative Molecular Field Analysis (CoMFA). 1. Effect of Shape on Binding of Steroids to Carrier Proteins. *J. Am. Chem. Soc.* **1988**, *110*, 5959−5967.

(22) Dewar, M. J. S.; Zoebish, E. G.; Healy, E. F.; Stewart, J. J. P. AM1: A new general purpose quantum mechanical molecular model. *J. Am. Chem. Soc.* **1985**, *107*, 3902−3909.
(23) Singh, U. C.; Kollman, P. A. An approach to computing electrostatic charges for molecules. *J. Comput. Chem.* **1984**, *5*, 129−145.
(24) Cornell, W. D.; Cieplak, P.; Bayly, C. I.; Gould, I. R.; Merz Jr., K. M.; Ferguson, D. M.; Spellmeyer, D. C.; Fox, T.; Caldwell, J. W.; Kollman, P. A. A second generation force field for the simulation of proteins, nucleic acids, and organic molecules. *J. Am. Chem. Soc.* **1995**, *117*, 5179−5197.
(25) Miertus, S.; Scrocco, E.; Tomasi, J. Electrostatic interaction of a solute with a continuum. A direct utilization of ab initio molecular potentials for the prevision of solvent effects. *Chem. Phys.* **1981**, *55*, 117−124.
(26) Miertus, S.; Tomasi, J. Approximate evaluations of the electrostatic free energy and internal energy changes in solution processes. *Chem. Phys.* **1982**, *65*, 239−245.
(27) Frisch, M. J.; Trucks, G. W.; Schlegel, H. B.; Gill, P. M. W.; Johnson, B. G.; Robb, M. A.; Cheeseman, J. R.; Keith, T. A.; Petersson, G. A.; Montgomery, J. A.; Raghavachari, K.; Al-Laham, A.; Zakrzewski, V. G.; Ortiz, J. V.; Foresman, J. B.; Cioslowski, J.; Stefanov, B. B.; Nanayakkara, A.; Challacombe, M.; Peng, C. Y.; Ayala, P. Y.; Chen, W.; Wong, W.; Andres, J. L.; Replogle, E. S.; Gomperts, R.; Martin, R. L.; Fox, D. J.; Binkley, J. S.; Defrees, D. J.; Baker, J.; Stewart, J. J. P.; Head-Gordon, M.; Gonzalez, C.; Pople, J. A. Gaussian 94; Gaussian, Inc.: Pittsburgh, PA, 1995.
(28) SYBYL; Tripos Inc., 1699 South Hanley Rd., St. Louis, MO 63144.
(29) Dunn, W. J. I.; Wold, S.; Edlund, U.; Hellberg, S.; Gasteiger, J. Multivariate Structure−Activity Relationship Between Data from a Battery of Biological Tests and an Ensemble of Structure Descriptors: The PLS Method. *Quant. Struct.-Act. Relat.* **1984**, *3*, 131−137.
(30) Wold, S.; Albano, C.; Dunn, W. J. I.; Edlund, U.; Esbenson, K.; Geladi, P.; Hellberg, S.; Johansson, E.; Lindberg, W.; Sjöström, M. Multivariate Data Analysis in Chemistry. In *Chemometrics: Mathematics and Statistics in Chemistry*; Kowalsky, B. R., Ed.; Reidel: Dordrecht, The Netherlands, 1984; pp 17−95.
(31) Levitt, M.; Perutz, M. F. Aromatic Rings Act as Hydrogen Bond Acceptors. *J. Mol. Biol.* **1988**, *201*, 751−754.
(32) Suzuki, S.; Green, P. G.; Bumgarner, R. E.; Dasgupta, S.; Goddard III, W. A.; Blake, G. A. Benzene Forms Hydrogen Bonds with Water. *Science* **1992**, *257*, 942−945.
(33) Burley, S. K.; Petsko, G. A. Aromatic−Aromatic Interaction: A Mechanism of Protein Structure Stabilization. *Science* **1985**, *229*, 23−28.
(34) Van Gunsteren, W. F.; Weiner, P. K.; Wilkinson, A. J. *Computer Simulation of Biomolecular Systems. Theoretical and Experimental Applications.*; ESCOM: Leiden, The Netherlands, 1993.
(35) Giraldo, J.; Martin, M.; Campillo, M.; Pardo, L. Theoretical studies of the histamine H_2-receptor: molecular mechanism of action of antagonists. *Mol. Pharmacol.* **1992**, *42*, 373−381.
(36) Mandel-Gutfreund, Y.; Margalit, H.; Jernigan, R. L.; Zhurkin, V. B. A role for CH···O interactions in Protein-DNA recognition. *J. Mol. Biol.* **1998**, *277*, 1129−1140.
(37) Chakrabarti, P.; Chakrabarti, S. C−H···O hydrogen bond involving proline residues in α-helices. *J. Mol. Biol.* **1998**, *284*, 867−873.
(38) Derewenda, Z. S.; Derewenda, U. The occurrence of C−H···O hydrogen bonds in proteins. *J. Mol. Biol.* **1995**, *252*, 248−262.
(39) Chakrabarti, P.; Samanta, U. CH/π interaction in the packing of the adenine ring in protein structures. *J. Mol. Biol.* **1995**, *251*, 9−14.
(40) Cruces, M. A.; Elorriaga, C.; Fernández-Alvarez, E.; Nieto, O. Acetylenic and allenic derivatives of 2-(5-methoxyindolyl)methylamine. Synthesis and evaluation as selective inhibitors of MAO-A and MAO-B. *Eur. J. Med. Chem.* **1990**, *25*, 257−265.
(41) Gómez, N.; Balsa, M. D.; Unzeta, M. A comparative study of some kinetic and molecular properties of microsomal and mitochondrial monoamine oxidase. *Biochem. Pharmacol.* **1988**, *37*, 3407−3413.
(42) Fowler, C. J.; Tipton, K. F. Concentration dependence of the oxidation of tyramine by the two forms of rat liver mitochondrial monoamine oxidase. *Biochem. Pharmacol.* **1981**, *30*, 3329−3332.
(43) Pérez, V.; Marco, J. L.; Fernández-Alvarez, E.; Unzeta, M. Relevance of benzyloxy group in 2-indolyl methylamines in the selective MAO-B inhibition. *Br. J. Pharmacol.* **1999**, *127*, 869−876.
(44) Walker, B.; Elmore, T. The irreversible inhibition of urokinae kidney cell plasminogen activator plasmin and B-trypsin by carbamoylimidazol. *Biochem. J.* **1984**, *221*, 277−280.
(45) Tabor, C. W.; Tabor, H.; Rosenthal. Purification of amine oxidases from beef plasma. *J. Biol. Chem.* **1954**, *208*, 644.
(46) Weissbach, H.; Smith, T. E.; Daly, T. W.; Witkop, B.; Underfriend, S. A rapid spectrophotometric assay of monoamine oxidase based on the rate of dissapareance of kynuramide. *J. Biol. Chem.* **1960**, *253*, 1160−1163.
(47) Cheng, Y. C.; Prusoff, W. H. Relationship between the inhibition constant (K_i) and the concentration of inhibitor which causes 50% inhibition (IC_{50}) of an enzymatic reaction. *Biochem. Pharmacol.* **1973**, *22*, 3099−3108.
(48) Kraulis, J. MOLSCRIPT: a program to produce both detailed and schematic plots of protein structure. *J. Appl. Crystallogr.* **1991**, *24*, 946−950.

JM991164X